Verification of a near-field error sensor placement method in active control of compact noise sources

Benjamin M. Shafer,[a] Kent L. Gee, and Scott D. Sommerfeldt
Department of Physics and Astronomy, N283 ESC, Brigham Young University, Provo, Utah 84602
bshafer@seriousmaterials.com, kentgee@byu.edu, scott_sommerfeldt@byu.edu

Abstract: Recent experiments in active noise control (ANC) have used near-field error sensors whose locations are determined according to the minimization of sound power. Sensors should be placed in regions where the sound pressure reductions are the greatest during sound power minimization of the ANC system. Near-field pressure measurements of noise sources with and without ANC were made. With the error sensors in theoretically ideal locations, the measured near-field pressure map approximates the theoretical map created under the condition of minimized radiated power. Moving the error sensors to theoretically nonideal locations greatly reduces the attenuation of radiated sound power.

PACS numbers: 43.28.Ra, 43.50.Ki [MS]
Date Received: September 28, 2009 **Date Accepted:** October 29, 2009

1. Introduction

Active noise control (ANC) strategies for small axial cooling fans have demonstrated that significant global sound power reduction in blade passage tones can be achieved. Early work in this area by Quinlan[1] and Lauchle *et al.*[2] has been followed by several recent studies.[3–8] A fundamental requirement for fan ANC to result in reduced sound power radiated by the fan is that the control sources be located close to the primary source relative to a wavelength. Near collocation of the sources yields source coupling and an alteration of the power radiated by the system of sources. Nelson *et al.*[9] described a process by which the radiated power by a collection of primary and secondary point sources may be minimized by optimizing the control complex source strengths. This solution becomes a theoretical limit to the control achievable in practice with real sources modeled appropriately as collections of monopoles.

Another important consideration in achieving global control is the locations of error sensors. An adaptive algorithm, such as a multichannel filtered-x least-mean-squared algorithm (e.g., see Ref. 10), is used to minimize the squared-pressure at the error sensors. The algorithm does not ensure that the global radiation is minimized, but rather searches for the best solution that minimizes the error signals. It stands to reason that the same minimum error sensor noise level achieved for different sensor configurations can result in changed reductions in radiated power. This is true because the control signal(s) generated to minimize the noise at the error sensors will vary according to error sensor placement, resulting in different source coupling.

Where then, should error sensors be placed to minimize the noise radiated, not just at the sensor locations, but everywhere? Some authors[11,12] place the error sensors in the acoustic far field of the primary source. Hansen and Snyder[13] advocated far-field error sensing techniques by arguing that far-field noise reductions are often associated with increases in near-field levels. However, others have investigated near-field sensing techniques[3,4,8,14,15] in some cases because a compact ANC system is deemed more practical.

---

[a]Author to whom correspondence should be addressed. Also at Serious Materials, 1250 Elko Dr., Sunnyvale, CA 94089.

This paper details the results of an experimental investigation that stems directly from the previous work of Gee and Sommerfeldt.[3,4] In their work, they devised a means by which they could place error sensors in the extreme near field of the primary and secondary sources. They modeled each source as an ideal monopole and employed the method of Nelson *et al.*[9] to obtain the secondary source strengths that resulted in minimum total radiated power. They reasoned that the ideal locations for error sensors would be the locations in which the sound pressure levels experienced the greatest reductions[13] for the condition of minimized radiated power. Plots of the radiated pressure fields from the primary and optimized secondary sources revealed near-field minima in the plane of the sources. They hypothesized that placement of the error sensors in these locations would cause the squared-pressure to be minimized there, thus causing the sources to be driven in such a way so as to result in significant sound power reductions. Although Gee and Sommerfeldt demonstrated that their error sensor placement strategy resulted in greater average far-field reductions with greater consistency (see Table 1 in Ref. 4), they did not directly establish the relationship between actual near-field pressure variations and far-field reductions achieved. This letter is an experimental validation of that error sensor placement method.

2. Experimental method

To guide error sensor placement, a tool was developed that allows the user to select configurations of primary and secondary point sources, find the secondary source strengths that minimize radiated power, and create spatial pressure maps to locate potential error sensor locations.[16] This tool has been used to efficiently investigate the error sensor placement and global reduction potential for many different types of source configurations.

The ANC apparatus used was similar to those employed by Gee and Sommerfeldt[3,4] and Monson *et al.*[8] To explore the effect of error sensor placement on global sound power attenuation, both near-field and far-field acoustic measurements were made in a fully anechoic chamber with working dimensions of $8.71 \times 5.66 \times 5.74$ m^3. The primary sources used were a 50-mm-diameter loudspeaker and a five-bladed 60-mm axial cooling fan. Each primary source was installed in the geographic center of near- and far-field measurement grids. The fundamental radiation frequency of both sources was 622 Hz, yielding dimensionless source sizes of $ka = 0.28$ for the loudspeaker and $ka = 0.34$ for the fan. The control sources used were four 25-mm loudspeakers symmetrically located as in Fig. 1(a).

To explore the effect of error sensor placement on global sound power attenuation, both near-field and far-field acoustic measurements were made. A linear near-field measurement array consisting of 23 type-I 6.35-mm prepolarized microphones, with a 12.7-mm intermicrophone spacing, mounted in a bracket along the measurement x-axis. The array traversed along the measurement y-axis in 6.35-mm increments, resulting in a total of 1058 measurement locations over a 20.3×28.6-cm^2 aperture. The linear near-field array is shown in Fig. 1(a). The far-field array measurement was a stepper-controlled measurement boom with 13 type-I 12.7-mm prepolarized microphones in a semicircular configuration and positioned in equal area segments for calculating sound power, as shown in Fig. 1(b). The boom array was initially positioned along the x-axis (refer to Fig. 1) and was rotated in 10° increments for a total of 234 measurements.

3. Measurement results

3.1 Loudspeaker near-field comparisons

For $ka = 0.28$, the loudspeaker primary source appeared to radiate essentially as a monopole source. When both the primary and control sources are treated as ideal monopoles and the geometrical configuration of the setup is input into the error sensor placement tool, the sound pressure level of the controlled field relative to the primary pressure field is shown in Fig. 2(a). What differentiates Fig. 2(a) from plots published in Refs. 4 and 8 is that the pressure fields in Fig. 2(a) are spatially averaged to approximate a 6.35-mm microphone measurement. This reduces the depth of the null that appears in between the sources (cf. Fig. 3 in Ref. 8) and shows that there are other locations in the near field outside the sources that can also lead to significant reductions, although they are not truly "ideal."

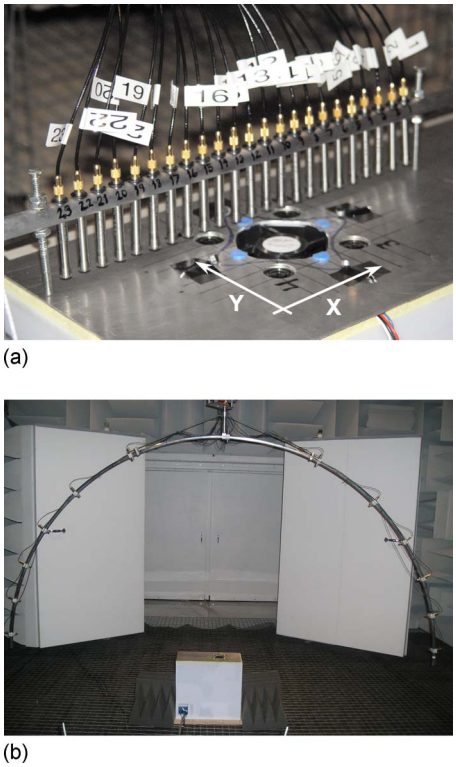

(a)

(b)

Fig. 1. (Color online) A photograph of (a) the linear near-field microphone array and aluminum plate used to install the primary and secondary sources, with white arrows and labels marking the directions of the *x*- and *y*-axes and (b) the angular far-field microphone array and noise source (bottom center).

Figures 2(b)–2(d) plot the near-field measurement of the loudspeaker and control actuators during ANC for three error sensor arrangements. Figure 2(b) shows the near-field sound pressure level relative to the primary field with ANC on and the four error sensors placed along the near-field null displayed in Fig. 2(a). The placement of the error sensors in these locations does, in fact, result in the desired coupling between the sources as evidenced by the similarity between Figs. 2(a) and 2(b). The region of closest resemblance is in and around the center of the primary source out to the locations of the control actuators. The variation between sound level reduction in Figs. 2(a) and 2(b) is greater outside of the primary source and control actuators. It is noted that the reduction near the ends of the measurement aperture was consistently less than the region in the vicinity of the sources for all tests and could be due to scattering and diffraction effects at the edges of the mock chassis.

In the test resulting in Fig. 2(c), one of the error sensors was removed from the theoretically ideal position and placed outside the sources where there should still be significant reductions. By comparing Figs. 2(b) and 2(c), this improved the control in the region to the right of the sources, while leaving the control achieved in the rest of the measured near-field region mostly the same. The variation in the sound level attenuation of Fig. 2(c) from the middle region of the theoretical map in Fig. 2(a) is greatest at the location of the theoretical pressure null to the right of the primary source.

In a more drastic test to examine the effects of error sensor placement on both near-field and global reductions, all four error sensors were placed in locations on the plate that were completely outside of any theoretically predicted pressure null. The near-field measurement for this error sensor placement, shown in Fig. 2(d), resulted in drastic changes in the near-field pressure when compared to Fig. 2(a). The common color scale reveals that although the sound

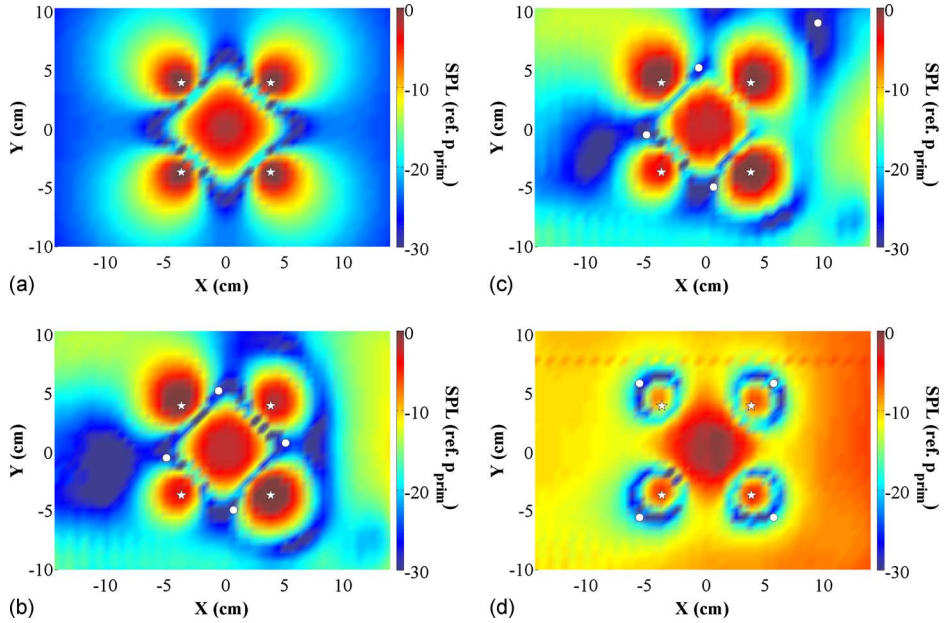

Fig. 2. (Color online) Near-field pressure maps (dB ref. 20 μPa) at 622 Hz—in a plane 0.6 cm above the source—of four-by-four ANC for (a) a theoretical point monopole and for the measurement of a 50-mm loudspeaker with (b) all error sensors placed in ideal locations, (c) three error sensors in ideal locations and one randomly placed, and (d) all error sensors in theoretical non-ideal near-field locations. Axis units are in centimeters. Circles and stars represent the locations of the error sensors and control actuators.

pressure level reduction is similar in the vicinity of the error sensors for both configurations, the average reduction in the near field is significantly greater with the microphones in theoretically ideal locations.

3.2 Far-field loudspeaker comparisons

The uncontrolled (wireframe) and controlled (surface) far-field sound pressure levels are shown in Fig. 3(a) for the loudspeaker primary source. The configuration corresponds to the near-field results shown in Fig. 2(b). In comparison, Fig. 3(b) shows the uncontrolled and controlled levels corresponding to the near-field results shown in Fig. 2(d). By moving the microphones to theoretically nonideal locations, not only is the near field significantly altered but there is a large difference in the sound power reductions achieved with the two configurations. With the error microphones in ideal locations [Fig. 3(a)], a sound power reduction of 17.1 dB was achieved.

With the error microphones in nonideal locations, the sound power was only reduced by 9.0 dB. These two results were obtained by averaging 12 trials, resulting in a standard deviation of 0.1 dB for both configurations. Not shown graphically are the angular sound pressure reductions for the configuration in Fig. 2(c), where one microphone was moved from the theoretically ideal location. Although there were some changes in the near-field and far-field sound pressure level patterns, the sound power reduction at 622 Hz was identical, 17.1 dB.

3.3 Near-field mapping and error sensor placement for an axial fan

A previous paper by Gee and Sommerfeldt[4] showed that greater global far-field reductions were achieved on average with the error microphones placed according to the theoretically ideal results of the near-field null mapping. To show that a near field similar to the theoretical field in Fig. 2(a) exists, the error sensor configuration in Fig. 2(b) was replicated for the 60-mm axial cooling fan used in Ref. 8. The near field of the axial fan without ANC was measured using the linear array and is shown in Fig. 4(a). This pressure map for 622 Hz indicates that the chassis-installed fan radiates similar to a monopole, but it is skewed in one direction.

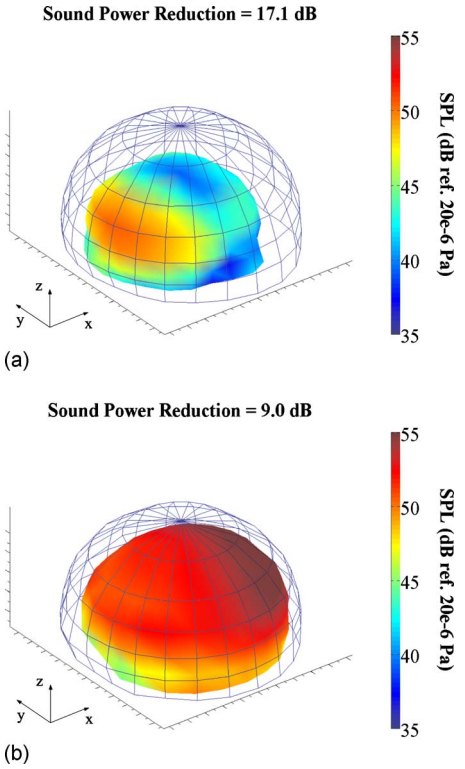

Fig. 3. (Color online) A far-field plot of the four-by-four ANC system when error sensors are located (a) according to theoretically predicted pressure nulls and (b) in theoretically non-ideal locations, with (color) and without (wire mesh) control for a 50-mm loudspeaker at 622 Hz. Axis units in dB ref. 20 μPa. The tick marks on the *z-axis* span from 0 to 55 dB (ref. 20×10^{-6} Pa). The center point on the *x*- and *y-axes* is 0 dB (ref. 20×10^{-6} Pa). The tick marks on each axis represent 5 dB (ref. 20×10^{-6} Pa).

Figure 4(b) is a measurement of the near field created by the fan and four 25-mm control loudspeakers during ANC and with each of the four error sensors placed in the same theoretically ideal locations as in Fig. 2(b). Although the overall shape of the near field resembles the theoretical prediction shown in Fig. 2(a), the nulls are not nearly as clearly accentuated as those measured for the loudspeaker in Fig. 2(b). This appears to be caused by the fact that the control at the blade passage frequency (BPF) is limited by the broadband noise floor of the fan. Nevertheless, the near field created is similar to that of the loudspeaker with the microphones in the same positions. For the sake of completeness, the sound power reduction for the fan, averaged over 12 trials, was 12.2 dB with a standard deviation of 0.3 dB.

4. Concluding discussion

The near-field measurements obtained during global ANC of a compact source have verified the error sensor positioning approach of Gee and Sommerfeldt.[4] In other words, placement of the error sensors in theoretically ideal near-field locations does, in fact, cause the adaptive control system to drive the control loudspeakers in such a way as to create the acoustic coupling that results in significant sound power reduction. Movement of the error sensors into nonideal locations can cause significant changes in the source coupling, and consequently, less attenuation in the near and far fields.

This is not to say that appreciable far-field attenuation cannot be achieved with the error sensors in theoretically nonideal locations. The modeling is based on mathematical monopoles; deviation of the sources from this behavior will cause some alteration of the near-field

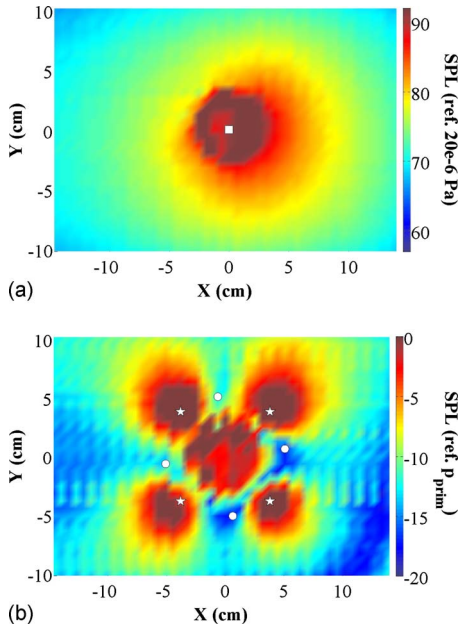

Fig. 4. (Color online) Measured near-field pressure maps at 622 Hz—in a plane 0.6 cm above the source—for (a) the 60-mm axial cooling fan without ANC (in dB ref. 20 μPa) and (b) the same fan and control actuators during four-by-four ANC (in dB ref. primary pressure field). The square marks the location of the source at the origin. Circles and stars represent the error sensors and control actuators. Note that the levels for the 2-cm radius circular region above the fan are contaminated by flow noise.

patterns. In addition, the finite widths of the error sensors will cause the region in which pressure is minimized to be somewhat different from the very thin nulls[4,8] predicted by theory. Thus, the method proposed by Gee and Sommerfeldt is useful as a systematic placement guide, but other error sensor locations [like the configuration in Fig. 2(c)] can also result in significant global reductions.

The approach of combining near-field and far-field measurements could be used as a diagnostic tool for a variety of ANC problems. In the case of the compact noise source, error sensor locations could be successively altered to demarcate regions in which global sound power reductions fall within a standard deviation of the ideal case. The near-field mapping could be used to understand in better detail the physics of the source coupling. Another possibility for this diagnostic technique would be to study the global control of noncompact noise sources. For example, although the axial fan appears to behave nominally as a monopole at the BPF, its radiation pattern will become more complex at higher harmonics. The noise source could be modeled with its multipolar characteristics and alternative ideal near-field locations sought analytically or numerically and verified experimentally.

References and links

[1]D. A. Quinlan, "Application of active control to axial flow fans," Noise Control Eng. J. **39**, 95–101 (1992).
[2]G. C. Lauchle, J. R. MacGillivray, and D. C. Swanson, "Active control of axial flow fan noise," J. Acoust. Soc. Am. **101**, 341–349 (1997).
[3]K. L. Gee and S. D. Sommerfeldt, "A compact active control implementation for axial cooling fan noise," Noise Control Eng. J. **51**, 325–334 (2003).
[4]K. L. Gee and S. D. Sommerfeldt, "Application of theoretical modeling to multichannel active control of cooling fan noise," J. Acoust. Soc. Am. **115**, 228–236 (2004).
[5]K. Homma, C. Fuller, and K. X. Man, "Broadband active-passive control of small axial fan noise emission," in Proceedings of the Noise-Con 2003 (2003), Paper No. nc03_206.
[6]Y.-J. Wong, R. Paurobally, and J. Pan, "Hybrid active and passive control of fan noise," Appl. Acoust. **64**, 885–901 (2003).
[7]J. Wang and L. Huang, "Active control of drag noise from a small axial flow fan," J. Acoust. Soc. Am. **120**,

192–203 (2006).
[8]B. B. Monson, S. D. Sommerfeldt, and K. L. Gee, "Improving compactness for active noise control of a small axial cooling fan," Noise Control Eng. J. **55**, 397–407 (2007).
[9]P. A. Nelson, A. R. D. Curtis, S. J. Elliot, and A. J. Bullmore, "The minimum power output of free field point sources and the active control of sound," J. Sound Vib. **116**, 397–414 (1987).
[10]S. D. Sommerfeldt, "Multi-channel adaptive control of structural vibration," Noise Control Eng. J. **37**, 77–89 (1991).
[11]A. J. Kempton, "The ambiguity of acoustic sources—A possibility for active control?," J. Sound Vib. **48**, 475–483 (1976).
[12]T. Martin and A. Roure, "Optimization of an active noise control system using spherical harmonics expansion of the primary field," J. Sound Vib. **201**, 577–593 (1997).
[13]C. H. Hansen and S. D. Snyder, *Active Control of Noise and Vibration* (E&FN Spon, London, 1997).
[14]A. Berry, X. Qiu, and C. H. Hansen, "Near-field sensing strategies for the active control of the sound radiated from a plate," J. Acoust. Soc. Am. **106**, 3394–3406 (1999).
[15]X. Qiu, C. H. Hansen, and X. Li, "A comparison of near-field acoustic error sensing strategies for the active control of harmonic free field sound radiation," J. Sound Vib. **215**, 81–103 (1998).
[16]S. D. Sommerfeldt and K. L. Gee, "Multi-channel active control system and method for the reduction of tonal noise from an axial fan," U.S. Patent No. 7,272,234 (September 18, 2007).